Research Reports

ALISSA: an automated live-cell imaging system for signal transduction analyses

Jakub Wenus[1]*, Heiko Düssmann[1]*, Perrine Paul[2], Dimitrios Kalamatianos[2], Markus Rehm[1], Peter E. Wellstead[2], Jochen H.M. Prehn[1], and Heinrich J. Huber[1]
[1]Department of Physiology & Medical Physics, Royal College of Surgeons in Ireland, Dublin, Ireland and [2]Hamilton Institute, National University of Ireland Maynooth, Maynooth, Ireland

BioTechniques 47:1033-1040 (December 2009) doi 10.2144/000113247
Keywords: automated microscopy; live cell imaging; image analysis; online event detection; apoptosis; software engineering

*J.W. and H.D. contributed equally to this work.
Supplementary material for this article is available at www.BioTechniques.com/article/113247.

Probe photobleaching and a specimen's sensitivity to phototoxicity severely limit the number of possible excitation cycles in time-lapse fluorescent microscopy experiments. Consequently, when a study of cellular processes requires measurements over hours or days, temporal resolution is limited, and spontaneous or rapid events may be missed, thus limiting conclusions about transduction events. We have developed ALISSA, a design framework and reference implementation for an automated live-cell imaging system for signal transduction analysis. It allows an adaptation of image modalities and laser resources tailored to the biological process, and thereby extends temporal resolution from minutes to seconds. The system employs online image analysis to detect cellular events that are then used to exercise microscope control. It consists of a reusable image analysis software for cell segmentation, tracking, and time series extraction, and a measurement-specific process control software that can be easily adapted to various biological settings. We have applied the ALISSA framework to the analysis of apoptosis as a demonstration case for slow onset and rapid execution signaling. The demonstration provides a clear proof-of-concept for ALISSA, and offers guidelines for its application in a broad spectrum of signal transduction studies.

Introduction

With the improvements in imaging technology and the ever-increasing number of novel probes, confocal time-lapse imaging has become a powerful tool for studies of living cells in biomedicine and systems biology (1–3). Today, synthetic fluorescent sensors can be applied to measure a number of different physiological parameters such as plasma and mitochondrial transmembrane potentials (4,5), ion concentrations (6,7), or intracellular pH (8,9). Likewise, cloned DNA can be introduced into cells to fluorescently label intracellular proteins of interest by marker proteins such as GFP, its spectral variants, and related fluorescent proteins (6,10). Employing fluorescent protein variants with different excitation/emission wavelengths, Förster (or fluorescence) resonance energy transfer (FRET) can be utilized to study protein-protein interactions, protein-DNA interactions, and protein conformational changes (11,12) within a living cell. Applications of the method range from drug toxicity studies (13) to investigations of biochemical signal transduction and its application to systems biology studies (14–16). However, single-cell studies such as cell proliferation (17,18) and studies of programmed cell death (apoptosis) pose a number of challenges to live cell imaging. Specifically, these studies may last up to several days because key signaling events often happen unpredictably or after a long lag period, but can then proceed rapidly once initiated (19,20). The long lag period produces a high and error-prone workload for the researcher as large image stacks have to be processed and stored. A more severe problem is posed by phototoxicity (2) and probe photobleaching (21), leaving the researcher with a limited sampling rate. This subsequently poses a trade-off between temporal resolution and maximum measurement time as imaging rates and setups are usually chosen at the beginning of the experiment. This dilemma is aggravated when the desired events are themselves rapid, but occur unpredictably and late after stimulus onset. Premature phototoxicity/photobleaching then limits the sampling rate and biological events may be entirely overlooked or resolved only at a temporal resolution that is too low. While there have been significant efforts to reduce these drawbacks by probe optimization (22,23), we present here a method that allows the economic use of laser excitation and imaging resources in a manner that is tailored to the stage of the experiment when they are required. Our approach employs cell segmentation, cell tracking, and time series evaluation online and in real time (e.g., during experimentation) to detect temporal onset of cellular events and change microscope image modalities subsequently. We present a software framework that separates process control from image analysis, rendering the latter reusable for a broad spectrum of applications. Proof-of-concept is provided by

applying the framework to signal transduction studies during apoptosis.

Materials and methods

Time-lapse microscopy and digital imaging

For the ALISSA proof-of-concept demonstration, cells were cultured in glass-bottom dishes (Cat. no. KIT-3512; Willco B.V., Amsterdam, The Netherlands) and equilibrated with 30 nM tetramethylrhodamine methyl ester (TMRM) in 4-(2-hydroxyethyl)-1-piperazineethanesulfonic acid–buffered (10 mM; pH 7.4) RPMI (both, Sigma-Aldrich, Arklow, Ireland) containing 10% FCS, covered with mineral oil, and placed in heated (37°C) incubation chambers (Tempcontrol Digital with Objective Heater and Heating Insert P; Carl Zeiss, Jena, Germany) that were mounted on the microscope stage. Apoptosis was induced with 1 μM staurosporine (STS) (Cat. no. ALX-380-014-M001; Alexis Corporation, Exeter, UK), a broad-spectrum kinase inhibitor. The confocal microscope used was a Zeiss LSM 510 META inverted microscope (Carl Zeiss) equipped with a 405-nm GaN laser, 488-nm argon laser, and a 543-nm helium/neon laser. Using a 63× 1.4 numerical aperture (N.A.) oil immersion objective, cyan fluorescent protein (CFP), FRET, yellow fluorescent protein (YFP), and TMRM fluorescence were measured using the appropriate filters and beam splitters. Acquisition channels and wavelengths are depicted in Table 1. Mitochondrial membrane potential depolarization accompanied by mitochondrial outer membrane permeabilization (MOMP) was detected by delocalization of the cationic fluorescent dye TMRM and using image analysis techniques as described in the "Time series extraction (IAS)" section. Cells were transfected with pCFP-DEVD-YFP construct to visualize effector caspase activity by FRET (24). Images were stored separately for each acquisition setting as 8-bit grayscale in TIFF format.

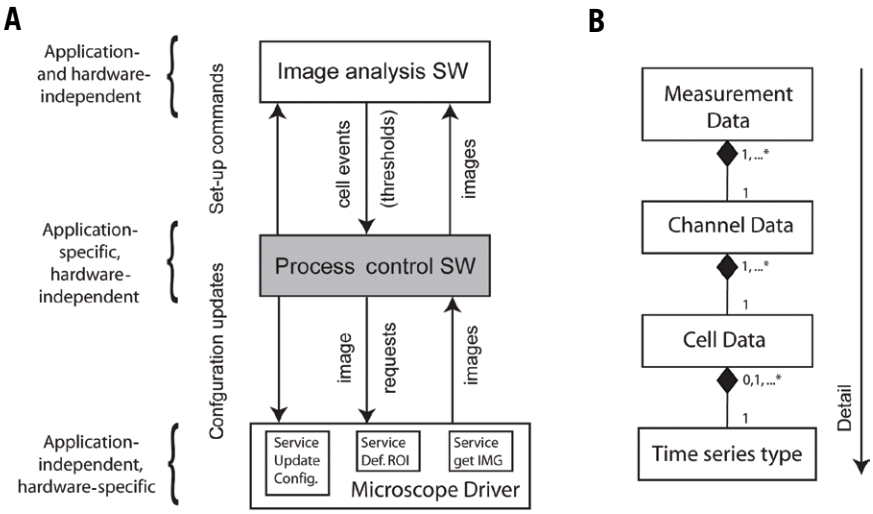

Figure 1. Framework and data structure for the automated live cell imaging system. (A) The entity diagram depicts the interworking among the PCS, IAS, and microscope driver. The PCS requests images from the microscope and passes the information to the IAS. Likewise, it sends commands to the IAS to request specific tasks, like threshold checks, that are reported back upon their detection. (B) UML diagram of the data structure used for data generation and threshold check. One dataset can contain one or more detection channels with data for each cell present. Data associated with each cell can have more time series types [pixel average $x(t)$ and pixel standard deviation $\sigma(t)$ are currently implemented in the IAS]. Thresholds can be requested by the PCS at each hierarchical level, and threshold events from the IAS are always channel-, cell-, and time series type–specific.

ALISSA architectural framework and building blocks

ALISSA is a modular software architecture for threshold-based automated live cell microscopy. To master the inherent complexity and to allow software re-use to the greatest extent, we created a software concept that separated microscope-specific software elements from the general structure elements that are independent of the actual hardware. Likewise, we also abstracted application-specific software that processes information about the signal transduction pathway from the application-independent image analysis elements. This resulted in three separate software entities as shown in Figure 1A: the biological context–independent and fully reusable Image Analysis Software (IAS), the biological context–dependent but hardware-independent Process Control Software (PCS), and the Microscope Driver (MD) as the only microscope-dependent software. The IAS is a MATLAB (version 2008a; The Mathworks, Cambridge, UK) code that performs cell segmentation, cell tracking, and time series extraction. It processes each image separately and has specific geometric information about cell localization, but requires no knowledge of the biological context and therefore is fully reusable for most signal transduction settings. The PCS controls the IAS, processes its information to decide on microscope control actions, and uses microscope-specific drivers for interacting with the hardware. Both entities—PCS and IAS—communicate via message exchange over a component object model (COM) interface for completion of common tasks. In the following sections, we describe the image processing methods and the PCS-IAS interworking guidelines for baseline computation and threshold detection. Subsequently, we provide an example implementation of the PCS illustrating the ALISSA framework for the process of apoptosis.

Cell segmentation (IAS)

Several classical segmentation algorithms were adapted and implemented. These comprise local maxima seeded watershed (25), circular seeded watershed (26), and modified constrained erosion-dilation (27) algorithms. In all cases, images are automatically pre-processed to remove noise and enhance contrast for segmen-

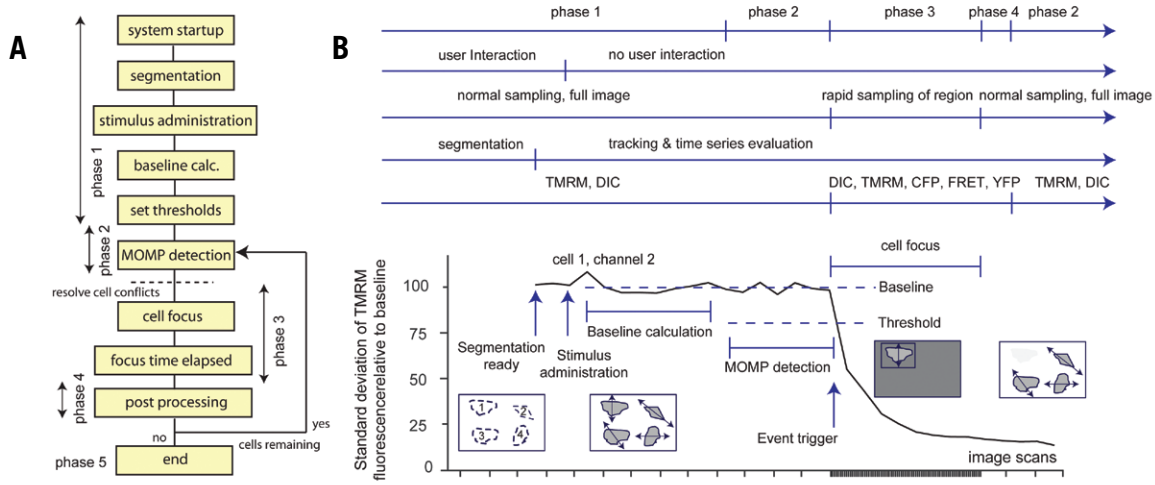

Figure 2. Overview over the application case–specific process control as described in the text. MOMP is detected for each cell as a change of the evidence signal relative to a stable baseline. Subsequently, a high-speed region scan is performed for that particular cell with additional laser channels to detect caspase activation. After scanning time has elapsed, the cell is discarded. Thresholding is resumed for the remaining cells after their viability has been checked in a post-processing procedure. (A) Flowchart-based view. (B) Time series–based view. Image processing and user interaction steps are exemplified for the time series of the average pixel intensity standard deviation in the TMRM channel and for subsequent focus on the cell in right top corner.

Table 1. Detection channels used in the application case

Channel number; name		Description	Excitation/emission (nm)	Laser	Reason for detection
1	DIC	Differential interference contrast	Transmission: 543	HeNe	S, T
2	TMRM	Sensor for mitochondrial polarization, MOMP	543 / >560	HeNe	S, T, E, B, D
3	YFP	Sensor for apoptosis execution (acceptor)	488 / 505 < λ < 550	Argon	S, E, B, D
4	FRET	Sensor for apoptosis execution (acceptor emission after FRET)	405 / 505 < λ < 550	GaN	E, B
5	CFP	Sensor for apoptosis execution (donor)	405 / 470 < λ < 500	GaN	E, B

While channels 1–2 are necessary for tracking and continuously active, channels 3–5 are only temporarily activated during rapid sampling and upon baseline calculation. Purposes of channels are segmentation (S), tracking (T), evaluation of time series (E), baseline calculation (B), and event detection (D).

tation purposes. As a key feature, these segmentation algorithms enable the parallel evaluation of several imaging channels that are generated by simultaneously measuring different cellular probes. After having chosen the best results, the user can edit the segmentation mask by manually drawing cell boundaries or discarding cells from analysis.

Cell tracking (IAS)

To follow the cell shapes during time-lapse imaging, two alternative methods are implemented that can be switched by the user at any time during an experiment. If the cell positions and shapes are not expected to change significantly over time, the initial segmentation mask can be applied at each image record. Alternatively, the cell shapes and positions are updated in real time for each new record. This is achieved by a tracking algorithm capable of using differential interface contrast (DIC) channel information only, in contrast to other reported solutions that require information on YFP or GFP images (28,29) and would thereby need high-energy laser excitation. Tracking is based on the condensation algorithm (30) in a manner that achieves robustness against noise and incompleteness in actual measurements on the DIC channel. To do so, the algorithm exploits assumptions of hypothetical cell movements and deformations from previous measurements by validating them against the actual measurements. More details on our implementation of the condensation algorithm can be found in the supplement. The DIC channel is first corrected for illumination using pseudo-flat field correction by dividing the image with the illumination trend computed using a large Gaussian kernel. DIC edges are then enhanced by automatic bi-level thresholding (31). For each record, cell boundary coordinates and polygonal bounding boxes are stored for further actions, such as selecting a region of interest. Tracking takes approximately 0.1 s per cell and is recorded using a 2.33 GHz processor with 2 GB RAM.

Time series extraction (IAS)

From the tracked cells over time, the IAS extracts fluorescence readouts for each channel and per cell; these are used as bases for thresholding and are stored in a database for further offline analysis. An overview over the data series structure obtained from each image is given in Figure 1B. For each detection channel and each cell, we calculated two types of time series: the mean pixel average $\chi(t)$ and the standard deviation $\sigma(t)$ of the fluorescent pixel intensity (16). The first is calculated by taking an average over each pixel value $x_i(t)$ inside the segmented cell:

$$\chi(t) = 1/N \sum_{i=1}^{N} x_i(t).$$

[Eq. 1]

The standard deviation (SD) of the average pixel intensity of dye fluorescence within the cells,

$$\sigma(t) = \sqrt{\frac{1}{N-1}\left(\sum_{i=1}^{N} x_i^2(t)\right) - \chi^2(t)}\ ,$$

[Eq. 2]

provides a mean for probe localization and can be calculated from the total number N and the intensity of the individual pixels $x_i(t)$ at certain times. As the SD value rapidly changes from high to low whenever proteins become more distributed, it provides a good indicator of compartmental release in cells (32). Finally, baselines are calculated by the image analysis software as a prerequisite for thresholding. In the current version of ALISSA, the baseline is computed using a moving average method. Therefore, for each cell, a mean of the last 30 records acquired until time t is compared with the value received at time t+1.

Microscope control

Microscope control is exercised via specific driver programs that allow updates of microscope configurations (Table 1), scans of region of interests, and adaptation of temporal sampling rates. Drivers have been established for Zeiss LSM510 and LSM-5Live that interface to the open-access Zeiss LSM5 VBA (Visual Basic for Applications) server. Likewise, drivers for the Zeiss LSM710, which follows a similar concept, are currently in development. Further details are found in the Supplementary Materials.

Biological event detection via signal thresholds

The following two sections introduce basic ALISSA concepts for the interworking of IAS and PCS with respect to threshold definition and detection, handling of setup conflicts, and synchronization of microscope and IAS after change of setup. They are described here on a conceptual level; further details are found in the Supplementary Materials, which also includes a catalog of messages and a message exchange diagram for the ALISSA example application described. Biological events are processed upon temporal changes of fluorescent probes that exceed or undergo predefined thresholds. These thresholds are defined by the user via graphical interfaces at the start of an experiment and stored in the PCS. They are specific for each cell and measurement channel, have a direction (exceed or underflow), and operate on the mean pixel average $\chi(t)$ or the standard deviation $\sigma(t)$ as defined above. Their values are percentages that are relative to stable baselines and are calculated by the IAS upon PCS request. The PCS then sends the threshold request including information of the required cell, measurement channel, direction, and type of time series [$\chi(t)$ or $\sigma(t)$] to the IAS. Actual values of $\chi(t)$ and $\sigma(t)$ per cell and channel are evaluated by the IAS and reported back to the PCS when a threshold occurs.

Event integration and conflict handling

As the IAS might report different thresholds for several cells at the same time, the PCS has to resolve conflicts to execute the right setup for the microscope. As a design principle, cells that are more downstream in a signal transduction cascade are given priority. For cells equally downstream, those where the actual signal is closer to the defined threshold value (i.e., the ones with a more recent event) are prioritized. After conflicts have been resolved, setup actions by PCS are initiated at the microscope. Such actions comprise increase of sampling rates, inclusion of new laser and filter resources, or may initiate a focus on the desired cell with potential magnification. Whenever changes of image modalities are involved, the PCS synchronizes microscope and IAS by using cell specific geometry information obtained from the IAS in the previous reporting threshold. Whenever a particular cell is in focus at the microscope, events of other cells cannot be detected and are checked later in a post-processing procedure.

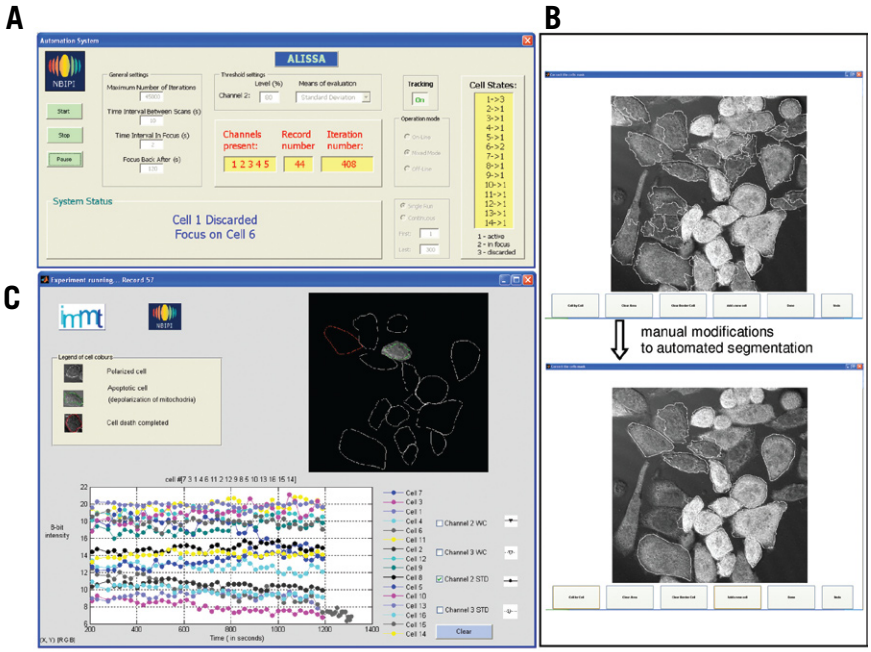

Figure 3. Graphical user interfaces. (A) PCS window displaying the initial system settings, number of active channels, number of the current image record, cell states, and the overall status of the experiment. (B) Results of applying one of the segmentation algorithms before (top) and after (bottom) manual modifications to the automated segmentation results. (C) IAS GUI in a state of logical focus on one of the cells where the mask border colors indicate cell states. White, active pre-apoptosis cells; red, cells discarded from analysis; green, the cell in focus.

Table 2. Control parameters as used in the process control example for mitochondrial apoptosis execution

Parameter	Value	Explanation
Initial sampling rate	1 scan per 45 s	Sampling rate before MOMP (phase 1 and 2)
Rapid sampling rate	1 scan per 15 s	Sampling rate after MOMP for given duration (region scan, phase 3)
Duration of rapid sampling	12 minutes	Phase 3 duration
Threshold detection channel	Channel 2, TMRM	Channel for which threshold is monitored (phase 2)
Time series type	Mean intensity $\chi(t)$	Value of cellular signal that is evaluated (see materials and methods, phase 2)
Value threshold detection	-20% of baseline	Changes of signal value according to baseline to establish trigger (phase 2)

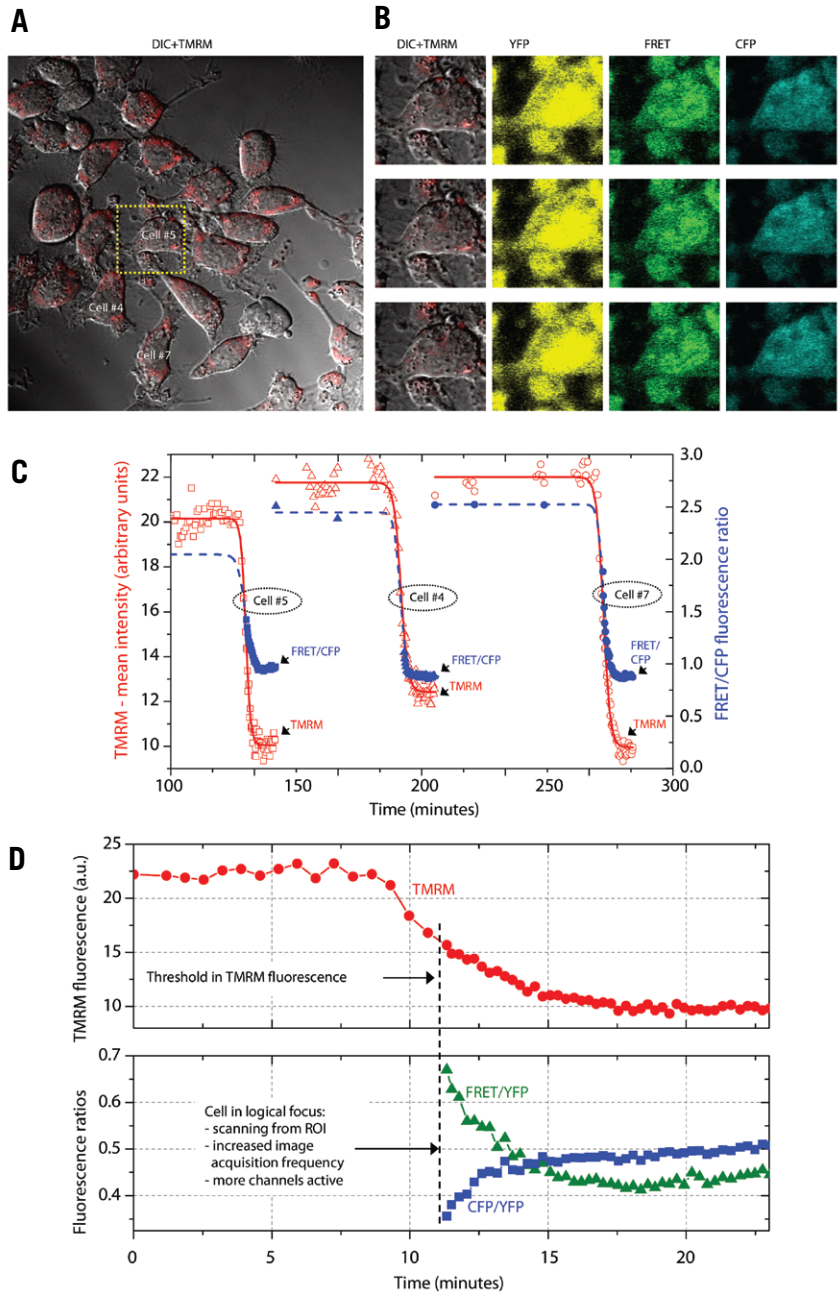

Figure 4. Automated processing of MOMP and effector caspases for the application case. (A) TMRM and DIC channel image for the experiment described in the main text highlighting three cells for further analysis (ALISSA internal numbering). For this image record, a threshold is detected for Cell #5 and a subsequent region scan around that cell is exercised (yellow dashed-line box). (B) Region scans for that cell with three consecutive records (rows) subsequent to the scan in (A). Columns depict scans for DIC/TMRM and further switched-on channels (YFP, FRET, CFP) as labeled. (C) Time series representing mean fluorescence intensities of TMRM (red color) and FRET/CFP ratio for the cells as labeled in (A) (blue color) for one experimental run. (D) Zoomed-in TMRM trace for Cell #7 (top panel) together with the corresponding FRET/YFP (green triangles) and CFP/YFP (blue squares) fluorescence ratios (bottom panel). Note the sampling rate subsequent to event detection which is depicted by sampling markers of both panels.

The exact synchronization protocol is found in the Supplementary Materials.

ALISSA demonstrator for apoptosis execution

To exemplify the ALISSA framework, we implemented an online process control software for the execution phase of programmed cell death (apoptosis). Apoptotic processes proceed through biochemical signal transduction cascades and can be studied by single cell microscopy using intra-cellular fluorescent probes. The mitochondrial pathway of apoptosis can be induced by several stimuli such as STS (20,33), leading to MOMP, the release of cytochrome c (34), and the activation of executioner caspases. Caspases are a family of cytosolic cysteine proteases that cleave cellular substrates. MOMP is accompanied by mitochondrial membrane depolarization, which can be measured by the distribution kinetics of charged fluorescence dyes like TMRM (4,16). Dye localization is often given by the standard deviation $\sigma(t)$ of the fluorescent pixel intensity (32), as described in the "Time series extraction (IAS)" section. Likewise, the activity of caspases can be detected using a recombinant CFP-DEVD-YFP fusion protein, which is cleaved by executioner caspases resulting in a FRET disruption in the whole cell. Since MOMP is a late and unpredictable event, but subsequent processes are rapid and biologically highly elusive, automated detection of MOMP and subsequent analysis of caspase-3 activation served as an ideal ALISSA demonstration case. This biological signal transduction sequence is translated into the software workflow of Figure 2A that operates on data series of fluorescent readout, as shown in Figure 2B. Pursuant with Figure 2A, we first employed DIC and TMRM channels to allow segmentation and tracking. Following manual stimulus administration, stable baselines are calculated as relative means for calculating thresholds. In the second phase prior to MOMP, only TMRM measurements are performed using the standard deviation of the average pixel intensity of the TMRM signal as evidence. After this signal has changed in a particular cell relative to a cell-specific baseline, MOMP onset is detected. In this third phase, the system activates further lasers to detect YFP, CFP, and FRET channels for caspase-3–induced cleavage of the FRET substrate. In addition, a region scan around the cell for a user-defined time is performed in a manner that allows an increase of the temporal sampling rate. After the specified time has elapsed, a brief post-processing is initiated to update image and channel information for all other cells. The process restarts from TMRM measurements to detect MOMP in subsequent cells. The PCS software is given as a Microsoft VBA macro as a plug-in to the Zeiss LSM5 VBA interfaces.

Third-party software dependency and data output

ALISSA uses MATLAB (version 2007b or newer) with Image Processing Toolbox and Statistics Toolbox. However, since MATLAB code can be compiled and deployed license-free as a standalone piece of software, no direct dependency to MATLAB is given. For our reference implementation, the Zeiss LSM5 macro libraries for instrument control must be further supported. Output time series

are provided as .csv files and the segmentation masks are stored as .bmp image data. Confocal images acquired during the system operation are stored in a standard Microsoft Access database format—.mdb—which is typically used by the Zeiss microscopes.

Results

Online setup and user input for the ALISSA demonstrator

We applied the ALISSA demonstrator to online measurements of HeLa cells exposed to STS. Cells were cultured, transfected, and plated as described in the "Materials and methods" section. TMRM was used as a reporter for detecting mitochondrial transmembrane potential depolarization. Cleavage of the CFP-DEVD-YFP fusion protein was used to report effector caspase activity by causing FRET disruption. The ALISSA demonstrator was started and images for all channels (Table 1) were retrieved from the microscope. In the control interface (Figure 3A), we selected a 45-s initial sampling rate and a 15-s rapid sampling rate that is applied upon event detection (Table 2). Likewise, we selected the event detection threshold to 20% loss of TMRM signal for mean intensity relative to its baseline, corresponding to a near-maximal cytochome c release (35). In the graphical user interface (GUI) for image analysis (Figure 3B), we chose the seeded watershed algorithm that was applied to the DIC and the TMRM image channel, by selecting respective GUI options. Likewise, we employed GUI features to discard border cells and cells with low segmentation from the analysis, and exercised the options to manually correct segmentation results for some cells (Figure 3B). After acknowledgment of the segmentation results, cell tracking was started using the DIC channel as described in the "Materials and methods" section. A tracking window that contains the segmentation mask overlaid on the DIC channel allowed detailed monitoring of cell-associated time series (Figure 3C). At the same time, the control GUI (Figure 3A) showed the cell states, active image channels, and the overall current status of the experiment. As a concluding user interaction, we added the stimulus STS.

ALISSA demonstrator applied to apoptosis signaling

In a typical experiment (Figure 4), 14 cells were successfully segmented and STS was added subsequently to induce apoptosis. After drug addition, the system detected MOMP and then exercised rapid sampling for 10 cells for the duration of 12 min in each case. Caspase activation, indicated by a systematic decrease in FRET signal, was clearly resolved for eight of 10 cells. Three other cells reported MOMP events during the rapid sampling procedure of other cells and could not be included in the analysis. One cell did not undergo MOMP during the 5-h experiment, while no necrotic cell death was observed.

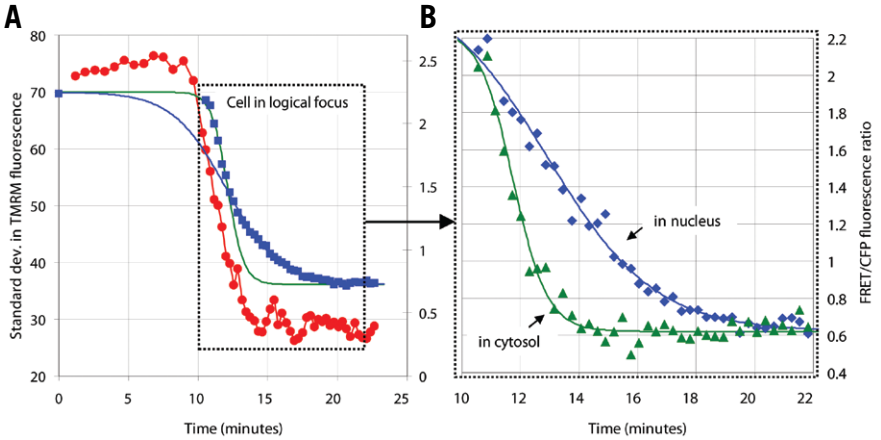

Figure 5. Bi-phasic decay in FRET/CFP fluorescence ratio shown with high temporal resolution. (A) Time series representing standard deviation in fluorescence intensity of TMRM (red circles) and FRET/CFP fluorescence ratio (blue squares). Two sigmoidal fits (solid blue and green lines) were necessary to render the biphasic behavior of caspase activation as obtained from high-speed measurements. (B) Dissection of the FRET/CFP fluorescence ratio from the cytosol (indicated by green triangles) from that of the nucleus (indicated by blue squares) for the cell shown in (A).

Figure 4, A and B demonstrates the results of the thresholding mechanism with an example cell indicated by the yellow dashed-line box at the time of threshold detection (Figure 4A). Region scans around that cell for three subsequent images with additional activated channels are depicted in Figure 4B. TMRM traces of MOMP detection for this and two further cells are shown in Figure 4C. Results of a typical event detection and subsequent rapid sampling with further detection channels are shown in Figure 4D. After the threshold based on the mean intensity of TMRM fluorescence was reported, fast changes in the FRET/YFP and FRET/CFP ratios were monitored by rapid sampling of the region around the cell. By monitoring with higher temporal resolutions, we were able to observe a biphasic decrease of the FRET/CFP ratio (Figure 5A) which was pronounced in some cells. We validated the hypothesis that this is due to different caspase activation kinetics in the nucleus and cytosol caused by limited diffusion, an effect that was suggested previously (16,36). This effect was further verified by separate evaluation of the CFP/FRET signal in the nuclear and cytosolic regions (Figure 5B), suggesting that ALISSA was able to temporally separate caspase activities in different cellular compartments.

Online measurements were repeated 25 times with different samples with the number of HeLa cells varying between 3 and 20 per sample. On average, using 80% drop of SD in TMRM fluorescence intensity as the threshold level value, thresholds were reported for 84% of the total number of segmented cells, while the remaining 16% of cells were healthy cells that did not report any threshold. For over half of the subpopulation with detected thresholds (51%), DEVDase activity–and therefore apoptosis–were correctly detected and recorded in region scans (43% of all initially segmented cells). A further 25% of this subpopulation was not taken into focus as their threshold events were received simultaneously with other cells (the reference implementation does not allow multiple region scans at the same time). The remainder of cells (24%) in the subpopulation with detected threshold, were actually falsely detected thresholds, mostly associated to cell tracking failure.

Discussion

ALISSA is a novel software framework that is ideally suited to perform automated live cell imaging. Its benefits range from automated segmentation and tracking, to adaptive change of image modalities, to online evaluation, which we have demonstrated here by way of a reference application. By switching on the high-energy lasers only for short time periods and within limited regions of interest, the total amount of laser radiation energy absorbed by the sample during experimentation is significantly lower when using ALISSA compared with conventional time-lapse imaging.

In previous studies (15,16,19,20) continuous FRET detection of effector

caspase activation using the LSM510 was recorded typically every 2 min (16) in the identical cellular system to avoid phototoxicity. In our current reference application, ALISSA was found to increase pre-event sampling (with low-energy lasers) to 45 s and post-event sampling (high-energy lasers for a short time) from minutes to 15 s. This rate is limited by two factors, (*i*) the actual speed of the microscope hardware, which takes about half of that time, and (*ii*) by the internal ALISSA processing. As the limiting rate is one of current technology and not one of methodology or phototoxicity, it is expected that microscope technological advancements, increased computer processing power, and the use of compiled computer languages such as C/C++ for image analysis will further improve ALISSA's performance.

Since the purpose of the reference implementation was to illustrate the concept and apply it to a standard confocal microscope, high efficiency of threshold detection was not prioritized. This is reflected in the fact that when cells were undergoing apoptosis simultaneously, only one cell was chosen for the high-frequency region scan, while the remaining cells were discarded from the analysis. In principle, the ALISSA framework—in particular, the interworking PCS-IAS protocol—does not pose such restrictions and would allow switching between two or more cells with simultaneous thresholding and region scans (at a cost of decreasing the temporal resolution). In favor of simplicity of the reference implementation, we reserved these more sophisticated applications for future studies.

ALISSA is not the first approach that combines image analysis with automation. Several approaches exist to perform cell counts (37), exercise autofocus and tracking (38), extract time series (39), and measure probe redistribution following photobleaching (40). These implementations are optimally suited to specific applications and are able to reduce mechanical workload, minimize phototoxicity and photobleaching, or increase spatial and/or temporal accuracy to gain biological insight. However, to allow software reuse to the greatest extent, ALISSA follows a different and more general approach by separating the design and software framework from the actual implementation while developing a detailed protocol of communication between the system entities. Using the well-established software engineering concepts of independent software layers (also known as orthogonalization of concerns) (41), we separated the image analysis from the process logic and established a novel interworking protocol for both entities. The image analysis is rendered as a reusable service program for cell segmentation, cell tracking, time series evaluation, and threshold detection. Tracing a signal transduction cascade via an automation system therefore becomes a matter of arranging existing building blocks on a logical level. This abstracts detailed geometric information while maintaining generality, thereby greatly facilitating the application of this technology to a broad spectrum of signal transduction studies and potentially even beyond. Examples are the study of apoptosis (19,20) as demonstrated here, the study of cell cycle events (18), or drug effects on respiration (42). Likewise, by separating the microscope drivers from the process logic, the system is suited for use with legacy equipment. The developed technology is applicable to all vendors that provide, or will provide, open application program interfaces (APIs) or software libraries able to control their hardware. In the present version, ALISSA uses VBA to access software libraries provided by Zeiss for control of their microscope. As a result, ALISSA currently integrates with Zeiss hardware, in particular with the LSM 510 and LSM 5Live, while portation to the Zeiss LSM710 is ongoing in our lab. Once other vendors provide similar control interfaces, ALISSA can be easily adapted with relatively simple modifications. Despite the current restrictive policy of some vendors to provide similar interfaces, experience from several industry sectors like process automation (43) suggest that vendors will provide open interfaces in response to market demand. To drive this demand, solutions like ALISSA are needed that require such open interfaces and that are broadly applied by the confocal microscopy community. By providing the framework, the interworking protocol, the image analysis, and a reference implementation to the academic community, we encourage the extension of the ALISSA concept. This may include the establishment of further microscope drivers in addition to the Zeiss LSM5 series used here, integrate novel image analysis features such as the analysis of cell morphology changes over time, three-dimensional segmentation, and three-dimensional tracking. Eventually, the ALISSA framework could help to develop standards for exercising control in single-cell signal transduction and cell fate studies.

Acknowledgments

The authors would like to thank Maximilian Wuerstle and Tytus Bernas for fruitful discussions. This research was supported by the National Biophotonics and Imaging Platform (HEA PRTLI Cycle 4; IMMT and ITC facilities), Science Foundation Ireland, Siemens IT Solutions, and the EU Framework Programme 7 (APO-SYS).

Competing interests

J.W., H.D., P.P., D.K., and H.H are coauthors for Irish Patent No. S20090230. M.R., P.E.W., and J.H.M.P. declare no competing interests.

References

1. **Bastiaens, P.I. and A. Squire.** 1999. Fluorescence lifetime imaging microscopy: spatial resolution of biochemical processes in the cell. Trends Cell Biol. *9*:48-52.
2. **Lichtman, J.W. and J.A. Conchello.** 2005. Fluorescence microscopy. Nat. Methods *2*:910-919.
3. **Pepperkok, R. and J. Ellenberg.** 2006. High-throughput fluorescence microscopy for systems biology. Nat. Rev. Mol. Cell Biol. *7*:690-696.
4. **Ehrenberg, B., V. Montana, M.D. Wei, J.P. Wuskell, and L.M. Loew.** 1988. Membrane potential can be determined in individual cells from the nernstian distribution of cationic dyes. Biophys. J. *53*:785-794.
5. **Scaduto, R.C., Jr. and L.W. Grotyohann.** 1999. Measurement of mitochondrial membrane potential using fluorescent rhodamine derivatives. Biophys. J. *76*:469-477.
6. **Tsien, R.Y.** 1998. The green fluorescent protein. Annu. Rev. Biochem. *67*:509-544.
7. **Tsien, R.Y.** 1989. Fluorescent indicators of ion concentrations. Methods Cell Biol. *30*:127-156.
8. **Matsuyama, S., J. Llopis, Q.L. Deveraux, R.Y. Tsien, and J.C. Reed.** 2000. Changes in intramitochondrial and cytosolic pH: early events that modulate caspase activation during apoptosis. Nat. Cell Biol. *2*:318-325.
9. **Llopis, J., J.M. McCaffery, A. Miyawaki, M.G. Farquhar, and R.Y. Tsien.** 1998. Measurement of cytosolic, mitochondrial, and Golgi pH in single living cells with green fluorescent proteins. Proc. Natl. Acad. Sci. USA *95*:6803-6808.
10. **Chalfie, M., Y. Tu, G. Euskirchen, W.W. Ward, and D.C. Prasher.** 1994. Green fluorescent protein as a marker for gene expression. Science *263*:802-805.
11. **Jares-Erijman, E.A. and T.M. Jovin.** 2006. Imaging molecular interactions in living cells by FRET microscopy. Curr. Opin. Chem. Biol. *10*:409-416.
12. **Jares-Erijman, E.A. and T.M. Jovin.** 2003. FRET imaging. Nat. Biotechnol. *21*:1387-1395.
13. **Perlman, Z.E., M.D. Slack, Y. Feng, T.J. Mitchison, L.F. Wu, and S.J. Altschuler.** 2004. Multidimensional drug profiling by automated microscopy. Science *306*:1194-1198.
14. **Albeck, J.G., J.M. Burke, B.B. Aldridge, M. Zhang, D.A. Lauffenburger, and P.K. Sorger.** 2008. Quantitative analysis of pathways controlling extrinsic apoptosis in single cells. Mol. Cell *30*:11-25.
15. **Rehm, M., H. Huber, C. Hellwig, S. Anguissula, H. Dussmann, and J. Prehn.** Dynamics of outer mitochondrial membrane permeabilization during apoptosis. Cell Death Differ. *16*:613-623.
16. **Rehm, M., H.J. Huber, H. Dussmann, and J.H. Prehn.** 2006. Systems analysis of effector caspase activation and its control by X-linked inhibitor of apoptosis protein. EMBO J. *25*:4338-4349.
17. **Kops, G.J., D.R. Foltz, and D.W. Cleveland.** 2004. Lethality to human cancer cells through massive chromosome loss by inhibition of the mitotic checkpoint. Proc. Natl. Acad. Sci. USA *101*:8699-8704.
18. **Lukas, J., C. Lukas, and J. Bartek.** 2004. Mammalian cell cycle checkpoints: signalling pathways and their organization in space and time. DNA Repair (Amst.) *3*:997-1007.
19. **Goldstein, J.C., N.J. Waterhouse, P. Juin, G.I. Evan, and D.R. Green.** 2000. The coordinate release of cytochrome c during apoptosis is rapid, complete and kinetically invariant. Nat. Cell Biol. *2*:156-162.
20. **Rehm, M., H. Dussmann, R.U. Janicke, J.M. Tavare, D. Kogel, and J.H. Prehn.** 2002. Single-cell fluorescence resonance energy transfer analysis demonstrates that caspase activation during apoptosis is a rapid process. Role of caspase-3. J. Biol. Chem. *277*:24506-24514.
21. **Zal, T. and N.R. Gascoigne.** 2004. Photobleaching-corrected FRET efficiency imaging of live cells. Biophys. J. *86*:3923-3939.
22. **Chen, Y., J.D. Muller, Q. Ruan, and E. Gratton.** 2002. Molecular brightness characterization of EGFP in vivo by fluorescence fluctuation spectroscopy. Biophys. J. *82*:133-144.
23. **Giloh, H. and J.W. Sedat.** 1982. Fluorescence microscopy: reduced photobleaching of rhodamine and fluorescein protein conjugates by n-propyl gallate. Science *217*:1252-1255.
24. **Tavare, J.M., L.M. Fletcher, and G.I. Welsh.** 2001. Using green fluorescent protein to study intracellular signalling. J. Endocrinol. *170*:297-306.
25. **Carpenter, A.E., T.R. Jones, M.R. Lamprecht, C. Clarke, I.H. Kang, O. Friman, D.A. Guertin, J.H. Chang, et al.** 2006. CellProfiler: image analysis software for identifying and quantifying cell phenotypes. Genome Biol. *7*:R100.
26. **Thomas, A.D., T. Davies, and A.R. Luxmoore.** 1992. The Hough transform for locating cell nuclei. Anal. Quant. Cytol. Histol. *14*:347-353.
27. **Adiga, P.S. and B.B. Chaudhuri.** 2000. Region based techniques for segmentation of volumetric histo-pathological images. Comput. Methods Programs Biomed. *61*:23-47.
28. **Shen, H., G. Nelson, D.E. Nelson, S. Kennedy, D.G. Spiller, T. Griffiths, N. Paton, S.G. Oliver, et al.** 2006. Automated tracking of gene expression in individual cells and cell compartments. J. R. Soc. Interface *3*:787-794.
29. **Zimmer, C., E. Labruyere, V. Meas-Yedid, N. Guillen, and J.C. Olivo-Marin.** 2002. Segmentation and tracking of migrating cells in videomicroscopy with parametric active contours: a tool for cell-based drug testing. IEEE Trans. Med. Imaging *21*:1212-1221.
30. **Isard, M. and A. Blake,** 1998. CONDENSATION—conditional density propagation for visual tracking. Int. J. Comput. Vis. *29*:5-28.
31. **Sezgin, M. and B. Sankur.** 2004. Survey over image thresholding techniques and quantitative performance evaluation. J. Electron. Imaging *13*:146-165.
32. **Ward, M.W., M. Rehm, H. Duessmann, S. Kacmar, C.G. Concannon, and J.H. Prehn.** 2006. Real time single cell analysis of Bid cleavage and Bid translocation during caspase-dependent and neuronal caspase-independent apoptosis. J. Biol. Chem. *281*:5837-5844.
33. **Tafani, M., D.A. Minchenko, A. Serroni, and J.L. Farber.** 2001. Induction of the mitochondrial permeability transition mediates the killing of HeLa cells by staurosporine. Cancer Res. *61*:2459-2466.
34. **Green, D.R. and G. Kroemer.** 2004. The pathophysiology of mitochondrial cell death. Science *305*:626-629.
35. **Dussmann, H., M. Rehm, D. Kogel, and J.H. Prehn.** 2003. Outer mitochondrial membrane permeabilization during apoptosis triggers caspase-independent mitochondrial and caspase-dependent plasma membrane potential depolarization: a single-cell analysis. J. Cell Sci. *116*:525-536.
36. **Maiuri, M.C., E. Zalckvar, A. Kimchi, and G. Kroemer.** 2007. Self-eating and self-killing: crosstalk between autophagy and apoptosis. Nat. Rev. Mol. Cell Biol. 8:741-752.
37. **Galbraith, W., M.C. Wagner, J. Chao, M. Abaza, L.A. Ernst, M.A. Nederlof, R.J. Hartsock, D.L. Taylor, and A.S. Waggoner.** 1991. Imaging cytometry by multiparameter fluorescence. Cytometry *12*:579-596.
38. **Rabut, G. and J. Ellenberg.** 2004. Automatic real-time three-dimensional cell tracking by fluorescence microscopy. J. Microsc. *216*:131-137.
39. **Chacko, A.D., N.T. Crawford, P.G. Johnston, and D.A. Fennell.** 2008. Machine vision based stochastic analysis of cancer cell mitochondrial dysfunction induced by a BH3 domain. Apoptosis *13*:1386-1393.
40. **Lippincott-Schwartz, J., E. Snapp, and A. Kenworthy.** 2001. Studying protein dynamics in living cells. Nat. Rev. Mol. Cell Biol. *2*:444-456.
41. **Keutzer, K., S. Malik, A. Newton, J. Rabaey, and A. Sangiovanni-Vincenti.** 2000. System-level design: orthogonalization of concerns and platform-based design. IEEE Trans. Comput. Aided Des. Integ. Circuits. *19*:1523-1543.
42. **Zhdanov, A.V., M.W. Ward, J.H. Prehn, and D.B. Papkovsky.** 2008. Dynamics of intracellular oxygen in PC12 Cells upon stimulation of neurotransmission. J. Biol. Chem. *283*:5650-5661.
43. **Mahnke, W., S. Leitner, and M. Damm.** 2009. OPC Unified Architecture. Springer-Verlag, Berlin.

Received 20 July 2009; accepted 22 September 2009.

Address correspondence to Heinrich Huber, Department of Physiology and Medical Physics, Royal College of Surgeons in Ireland, RCSI York House, York Street, Dublin, Ireland. email: heinhuber@rcsi.ie.